ACS APPLIED POLYMER MATERIALS

pubs.acs.org/acsapm

Forum Article

Selective Swelling of Stretched Block Copolymer Hollow Fibers for Upgraded Membrane Performance

Dinglei Zhong, Shoutian Qiu,* Jiemei Zhou, Dongwei Ma, and Yong Wang*

Cite This: *ACS Appl. Polym. Mater.* 2022, 4, 7989−7997

Read Online

ACCESS | Metrics & More | Article Recommendations | Supporting Information

ABSTRACT: Block copolymers are showing great potential in the preparation of advanced membranes for precise separations, and there is a strong interest in the development of hollow-fiber membranes (HFMs) from block copolymers. Herein, we report polysulfone-*block*-poly(ethylene glycol) (PSF-*b*-PEG) HFMs with enhanced separation performance prepared by a convenient stretching strategy. Axial stretching is first applied to the melt-spun PSF-*b*-PEG hollow fibers, efficiently reducing the wall thickness and outer diameter of the hollow fibers. The stretched hollow fibers are then subjected to selective swelling, thus producing HFMs with interconnected nanoporosity. We find that the degree of stretching significantly influences the diameter, length, and separation performance as well as the crystallization behavior of the hollow fibers before and after selective swelling. With a stretching percentage of 527%, the HFMs exhibit simultaneously enhanced water permeance and rejection because of thinned fiber walls and reduced pore sizes. This work reveals the important role of axial stretching in upgrading the performance of block copolymer HFMs and demonstrates that the selective swelling coupled with melt spinning is promising in the cleaner preparation of HFMs.

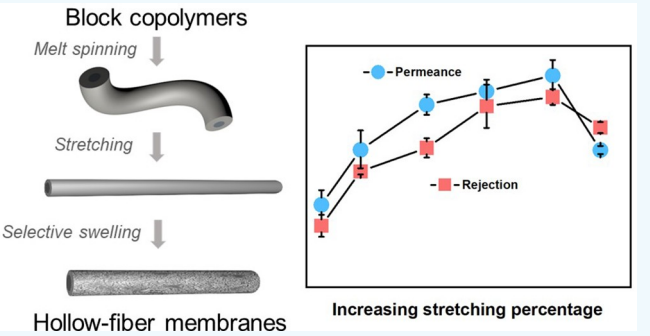

KEYWORDS: *stretching, hollow-fiber membranes, selective swelling, block copolymers, performance upgrade*

1. INTRODUCTION

Hollow-fiber membranes (HFMs) with the excellent mechanical strength, high packing densities, and a self-supporting nature have been extensively used in water treatment, gas separation, and biomedicines.[1−6] Currently, three main methods prevail for the large-scale fabrication of polymeric HFMs, i.e., thermally induced phase separation (TIPS),[7−9] solution spinning through nonsolvent induced phase separation (NIPS),[10−12] and melt spinning and stretching.[13−15] However, during the manufacturing process of NIPS and TIPS, polymers together with additives are dissolved in solvents or diluters, and this process relies heavily on toxic solvents and produces massive wastewater.[16] In contrast, the preparation of HFMs by melt spinning and cold stretching is based on the theory of lamellae separation and, thus, is only applicable to crystalline polymers such as polypropyene (PP), polyethylene (PE), and polyvinylidene fluoride (PVDF).[14,15,17,18] HFMs prepared by this method usually exhibit strong mechanical properties; however, low porosity and poor pore connectivity caused by stretching may result in low permeance.[17,19]

In the past decade, with the ever-increasing concerns and stringent regulations on environmental safety, the clean production of membranes using sustainable processes has been listed in the top priorities for the development of next-generation membranes. In this situation, melt spinning without solvents is undoubtedly emphasized. More recently, we reported a facile, efficient, and environmental-friendly strategy for the fabrication of ultrafiltration HFMs with well-defined porosities by selective swelling of melt-spun block copolymer hollow fibers.[20] Hollow fibers of polysulfone-*block*-poly(ethylene glycol) (PSF-*b*-PEG) with dense fiber walls were prepared via a continuous melt spinning process in which no organic solvent was required. Afterward, selective swelling, a facile yet efficient pore-forming method, was used to create nanoporosity in the hollow fibers.[21−23] As a result, HFMs with tunable pore sizes and separation performance were formed along with PEG chains enriched on the membrane surface.[24] However, HFMs manufactured by this process of coupling melt spinning with selective swelling only deliver a relatively low water permeance and rejection because of their symmetrical structure and large wall thickness.

In the manufacturing of hollow fibers, mechanical stretching in the melt state is often utilized to adjust fiber dimensions and

Special Issue: Polymer Membranes for Precision Separations

Received: December 22, 2021
Accepted: March 29, 2022
Published: April 13, 2022

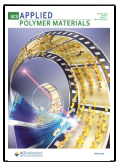

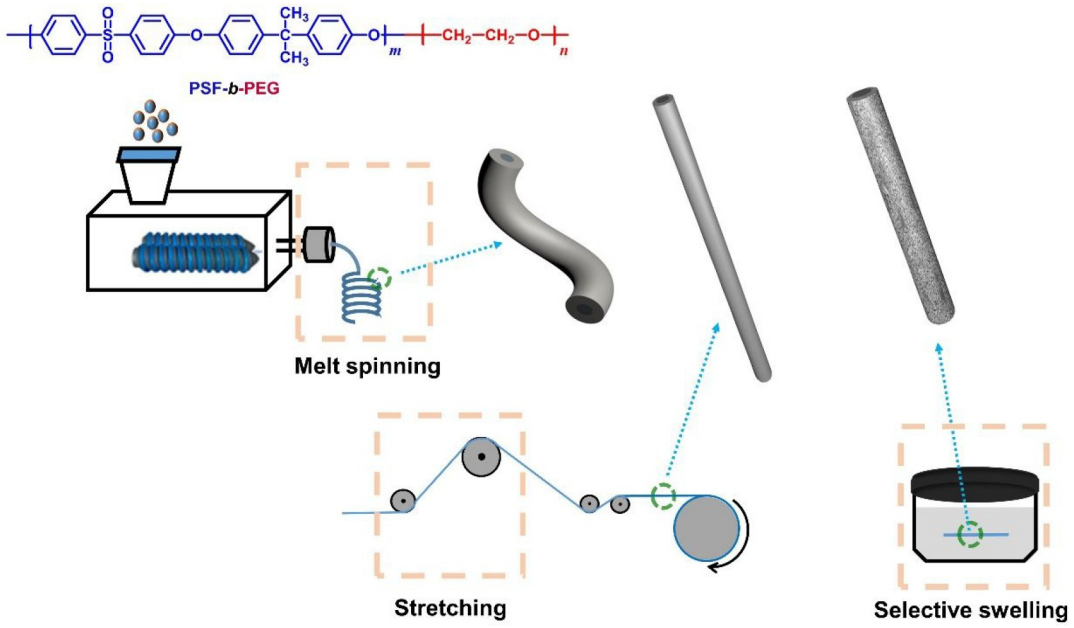

Figure 1. Schematic diagram for the preparation of PSF-*b*-PEG HFMs by melt spinning, stretching, and selective swelling.

modify fiber strength.[25] Furthermore, stretching usually improves the orientation degree and crystallinity of crystalline polymers and consequently the mechanical properties. This is predominantly attributed to molecular chains oriented along the direction of tension during the extrusion and stretching process.[26,27]

Considering the strong effect of stretching in changing the dimensions and the separation performance of hollow-fiber membranes, we expect that stretching may also play a positive role in upgrading the performance of PSF-*b*-PEG HFMs as it can greatly reduce the wall thickness and thus increase water permeance. Unlike the crystallizable polymers described above, PSF-*b*-PEG represents a two-phase structure in which the majority PSF block is an amorphous polymer while the minority PEG block can crystallize. Thus, during the stretching process, the matrix formed from the amorphous but rigid PSF may have a significant impact on the crystallization of the flexible PEG block.[28] Besides, the swelling behavior of the oriented molecular chains caused by stretching in selective solvents is also unclear. Thus, in this work, stretching is introduced to the melt-spun PSF-*b*-PEG hollow fibers followed by selective swelling in order to regulate the initial membrane dimensions as well as membrane thickness and consequently to improve the separation performance of the HFMs.

2. EXPERIMENTAL SECTION

2.1. Materials. PSF-*b*-PEG block copolymer with a PEG weight ratio of 21% was obtained from Nanjing Bangding. The PEG block had a molecular weight of ~20 kDa while the polydispersity index of the copolymer was ~2.00.[29] PEG homopolymer with a molecular weight of 20 kDa was obtained from Aladdin. Acetone (Ac; >99.5%) was purchased from Sinopharm while *n*-propanol (Pa; >99.0%) and *n*-heptane were obtained from Aladdin. Phosphate-buffered saline (PBS) tablets as well as bovine serum albumin (BSA; 98%, M_w = 66 kDa) were supplied by MP Biomedicals. All reagents were used as received. Deionized water with a conductivity of 8−20 μS·cm^{-1} was used in all tests.

2.2. Preparation of PSF-*b*-PEG Hollow-Fiber Membranes by Stretching and Selective Swelling. The PSF-*b*-PEG hollow fibers were prepared by melt spinning using a twin screw microextruder (Xinshuo, WLG10G). Figure 1 shows the schematic diagram of the preparation process. The size of the spinneret equipped to the extruder was $D/d_1/d_2$ = 0.5/0.28/0.15 mm, where D and d_1 are the outer and inner diameter of the annular orifice in the spinneret and d_2 represents the diameter of the inner channel, and the orifice gap was 110 μm. During melt spinning, the molding temperature was set at 200 and 210 °C for the upper and lower cavity of the extruder, respectively. Nitrogen was used as a protection gas. Without additional stretching, hollow fibers were spun at a speed of 75 mm·min^{-1}. When stretching was applied to nacent hollow fibers after melt spinning, the spinning speed was increased to 85−550 mm·min^{-1}. The stretching percentage (%) of hollow fibers was calculated by eq 1:

$$\text{stretching percentage} = \left(\frac{v_s}{v_0} - 1\right) \times 100\% \quad (1)$$

where v_s (mm·min^{-1}) represents the spinning speed with stretching and v_0 (mm·min−1) represents the initial spinning speed of the hollow fiber without stretching. In this work, v_s is always higher than v_0, and v_0 was fixed at 75 mm·min^{-1}. On the basis of the stretching percentage, the stretched hollow fibers were denoted as HF-*X* (*X* represents the corresponding stretching percentage). Herein, as-spun hollow fibers with spinning speeds varied from 75 to 550 mm·min^{-1} were labeled as HF-0%, -13%, -100%, -247%, -380%, -527%, and -633%.

For selective swelling, the PSF-*b*-PEG hollow fibers with different stretching percentages were immersed in the mixture of 80% Pa + 20% Ac (w/w) at 65 °C for 1 h and were then subjected to post-treatment and dried at 40 °C for 1 h until reaching a constant weight.[20,24] The thus-obtained HFMs were denoted as HFM-*X*, where *X* was the corresponding stretching percentage. The membranes after selective swelling were accordingly named HFM-0%, -13%, -100%, -247%, -380%, -527%, and -633%.

2.3. Characterizations. The surface and cross-sectional morphologies of the PSF-*b*-PEG hollow fibers before and after swelling treatment were observed on a scanning electron microscope (SEM; Hitachi S4800). The samples were immersed in liquid nitrogen and fractured immediately after being soaked in isopropanol so as to expose the cross sections of the samples. The inner surface of the hollow fibers and HFMs was exposed by lengthwise cutting, while the outer surface was tested directly. Before the morphology characterization, all samples were coated with a thin layer of platinum by an ion sputter (Hitachi MC1000) under vacuum at the sputtering current of

https://doi.org/10.1021/acsapm.1c01882
ACS Appl. Polym. Mater. 2022, 4, 7989−7997

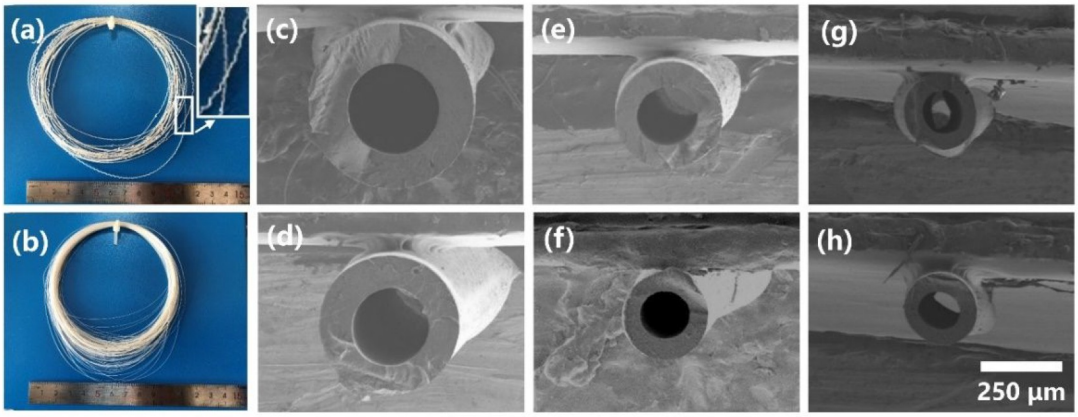

Figure 2. Photographs of (a) HF-0% and (b) HF-527% and cross-sectional SEM micrographs of the PSF-*b*-PEG hollow fibers with different stretching percentages: (c) HF-13%, (d) HF-100%, (e) HF-247%, (f) HF-380%, (g) HF-527%, and (h) HF-633%. (c–h) Same magnification and the scale bar is given in (h). Inset in (a) highlights the wavy structure of the hollow fiber.

15 mA for 15 s to enhance the conductivity of the sample. The surface porosities of the HFMs were analyzed by ImageJ. The thermogravimetric analysis of PSF-*b*-PEG was investigated by a synchronous thermal analyzer instrument (NETZSCH, STA 449 F3) under nitrogen with a constant flow rate of 20 mL·min^{-1}. The weight of the sample was around 15 mg. The heating trace was performed from room temperature up to 800 °C with a heating rate of 10 °C·min^{-1}.

The crystallization and melting behaviors of the PEG homopolymer, PSF-*b*-PEG copolymer, as well as the stretched hollow fibers and HFMs were investigated by a differential scanning calorimeter (DSC) instrument (TA, Q20). The weights of the samples were around 5–10 mg. The melting behaviors were examined at a scanning rate of 10 °C·min^{-1} from −40 to 100 °C. The crystallization behavior of the PEG homopolymer was cooled to −40 °C at 10 °C·min^{-1} after annealing at 100 °C for 3 min. All the procedures were conducted under a nitrogen atmosphere. The crystallinity of PSF-*b*-PEG hollow fibers was calculated by eq 2:

$$\text{crystallinity} = \frac{\Delta H_m}{f_{PEG}\,\Delta H_m^0} \times 100\% \tag{2}$$

where ΔH_m (J·g^{-1}) is the melting entropy of the PEG blocks in the PSF-*b*-PEG block copolymer and the stretched hollow fibers, while ΔH_m^0 (J·g^{-1}) represents the heat enthalpy of melting the PEG homopolymer with 100% crystallinity and was taken as 220 J·g^{-130}. f_{PEG} represents the weight ratio of the PEG block in the PSF-*b*-PEG copolymer.

2.4. Filtration Tests. Pure water permeance (PWP) and retention performance of HFMs were tested on a filtration apparatus working in the cross-flow mode. In the tests, HFMs were sealed in a polyurethane tube (8 × 12 mm) by the hot-melt adhesive and prepressed at 2 bar for 10 min before testing. The HFMs were tested at a stable pressure of 2 bar. The PWP was calculated by eq 3:

$$\text{PWP} = \frac{V}{\pi \times d \times l \times t \times \Delta P} \times 100\% \tag{3}$$

where PWP (L·m^{-2}·h^{-1}·bar^{-1}) represents the pure water permeance of the HFMs. d (m) and l (m) are the outer diameter and the effective length of the tested HFMs, respectively. t (h) is the testing time, and ΔP (bar) is the operation pressure, while V (L) is the volume of pure water passing through the HFMs.

In the rejection tests, BSA was dissolved in the aqueous PBS solution, producing a BSA solution with a concentration of 0.5 g·L^{-1}. The rejection tests were performed at 25 °C, and the BSA concentrations were determined via a UV–vis spectrometer (Thermo Scientific, NanoDrop 2000C) at the wavelength of 280 nm. The BSA rejection (R, %) was then calculated by eq 4:

$$R = \frac{C_f - C_p}{C_f} \times 100\% \tag{4}$$

where C_f and C_p are the BSA concentration (g·L^{-1}) in the feed and permeate, respectively.

3. RESULTS AND DISCUSSION

3.1. Stretching of Melt-Spun PSF-*b*-PEG Hollow Fibers. PSF-*b*-PEG, composed of the high-strength PSF block and the flexible PEG block, is suitable for melt spun and stretching and can be cavitated by selective swelling.[24] The hollow-fiber membranes prepared by melt spinning and selective swelling exhibited excellent tensile strengths.[20] Besides, this block copolymer (BCP) is also available at large scale; therefore, PSF-*b*-PEG was chosen as a promising material and studied in this work. The nascent hollow fibers obtained by melt spinning, which will be stretched at different rates in this study, require the melt of PSF-*b*-PEG to have strong fluidity to ensure that no fracture occurs during the high-speed tensile process. In order to avoid the oxidation of the PEG block, thermogravimetry was employed to characterize the thermal stability of PSF-*b*-PEG. As shown in Figure S1, PSF-*b*-PEG began to degrade at around 400 °C in nitrogen, which determined the upper heating limit of the spinning process. Thus, after multiple attempts and systematical investigation, 200/210 °C with nitrogen as the protective atmosphere was selected as the processing temperature. In this case, the initial spinning speed reached a high value at 75 mm·min^{-1}, which is 5 times that reported in our previous work, significantly enhancing the production efficiency of the melt spinning process.[20] In addition, as shown in Figure S2, all the spun PSF-*b*-PEG hollow fibers showed a light brownish color similar to that of the BCP granules, implying that the blanket of 2 L·min^{-1} nitrogen effectively avoids the oxidation of the copolymer even when spinning at such a high temperature. This color change is consistent with the thermogravimetric result.

Importantly, when the melting temperature reached 200/210 °C, the molten polymer exhibited excessive fluidity and underwent melt fracture during the extrusion process. Consequently, the obtained hollow fibers showed a wavy structure (Figure 2a). However, as illustrated in Figure S2a, by means of a simple stretching process, smooth and straight

https://doi.org/10.1021/acsapm.1c01882
ACS Appl. Polym. Mater. 2022, 4, 7989–7997

hollow fibers were easily obtained even at a stretching rate slightly higher than the melt extrusion rate (e.g., 85 mm·min^{-1}). With the progressive increase in the stretching percentages, the diameters of the fibers were gradually decreased. The hollow structure and smooth surface still remained, even when the stretching percentage reached 633%, verifying that PSF-*b*-PEG has excellent fluidity and processability under the current conditions. Considering that the corrugated structure of the as-spun hollow fibers without stretching, i.e., HF-0%, is not suitable for subsequent experiments and performance tests, we will only discuss the stretched hollow fibers in the following part of this work.

To further investigate the effect of stretching on the dimensions and morphologies of the hollow fibers, we systematically studied the surface and cross-sectional morphology of hollow fibers with different stretching percentages by SEM. As can be clearly observed from Figure S3a–f, despite a small number of globular structures on the surface, the hollow fibers subjected to stretching with various stretching percentages all represented a smooth and dense surface. In addition, as a result of the orientation effect caused by stretching, the dimensions of PSF-*b*-PEG hollow fibers were obviously decreased with the increasing stretching percentages. As can be seen clearly from Figure 2, with the constantly enhanced stretching percentages from 13% to 633%, the outer diameter of the stretched hollow fibers was decreased from 508 to 221 μm, and the inner diameter was reduced from 276 to 135 μm; the wall thickness descended from 116 to 43 μm. All the detailed data on the dimensions of the hollow fibers subjected to stretching with different ratios are listed in Table 1. The results indicated that stretching effectively reduced the wall thickness of the hollow fibers, which is highly desired for the sake of improving the water permeance of HFMs.[20] Meanwhile, an integral hollow structure and dense cross section were observed for all hollow fibers stretched at various stretching percentages. Even at a stretching percentage as high as 633%, the hollow fiber maintained its structural integrity and no cracks or cavity can be observed on its surface or in the cross section (Figure S3f,l). Therefore, we understand that stretching is herein a very simple and effective method to reduce the wall thickness and dimensions of the PSF-*b*-PEG hollow fibers, which will further improve the production efficiency and simultaneously enhance the performance of the PSF-*b*-PEG HFMs.

Table 1. Dimension Parameters of the PSF-*b*-PEG Hollow Fibers with Different Stretching Percentages

samples	outer diameter/μm	inner diameter/μm	wall thickness/μm
HF-13%	508	276	116
HF-100%	437	240	99
HF-247%	327	189	69
HF-380%	265	151	57
HF-527%	237	136	51
HF-633%	221	135	43

3.2. Selective Swelling of Stretched Hollow Fibers.

Selective swelling was then performed on stretched hollow fibers to generate interconnected porosities throughout the fiber walls, thus producing HFMs following the mechanism of selective swelling-induced pore generation. During the swelling process, molecular chains interact strongly with the swelling agent and possess enhanced segmental mobility, which will have a significant influence on the hollow fibers. Typically, the length of PSF-*b*-PEG hollow fibers was changed significantly after selective swelling. As shown in Figure 3a, for the fiber with a small stretching percentage of only 13%, its length after swelling was increased by 18.9%. With rising stretching percentages, the increasing rates of the fiber lengths were dramatically declined after selective swelling. Notably, for hollow fibers with the stretching percentage exceeding 150%, their lengths were even shortened. For the hollow fiber with the stretching percentage of 633%, its length was decreased by 37.9% after swelling. Obviously, there was a negative correlation between the length changing rate and the stretching percentage. This should be attributed to the competing effect of size expansion caused by selective swelling and length recovery as a result of relaxation of the oriented chains under the condition of selective swelling. In the absence of external force, the polymer chains were randomly entangled in the as-synthesized BCPs, and the arrangement of the polymer chains had no preferable direction of orientation. By means of extruding and stretching, the polymer chains were changed from a random entanglement state to a directional orientation. The degree of chain packing and orientation is generally increased with increasing stretching percentages. After melt

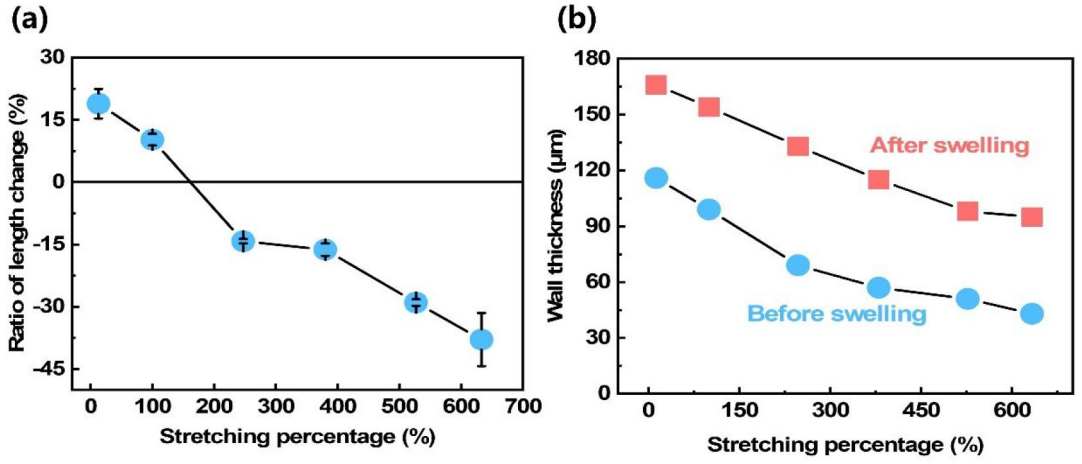

Figure 3. (a) Ratio of length change and (b) wall thickness to stretching percentage of PSF-*b*-PEG hollow fibers before and after swelling.

https://doi.org/10.1021/acsapm.1c01882
ACS Appl. Polym. Mater. 2022, 4, 7989−7997

extrusion, the neat orientation was maintained as the molecular chains went through a rapid cooling process. However, in the process of the swelling treatment, the swelling agent strongly swelled the PEG minority domains and moderately swelled the PSF matrix because of the affinity between the agent and the two blocks. As a result, the volume of hollow fibers was expanded to accommodate the strongly swelled PEG phases. After evaporation of the swelling agent at room temperature, the expanded PSF framework was frozen as PSF chains lost their mobility to deform while PEG chains collapsed, leading to interconnected porosity with PEG chains lined along the pore walls and surface. With the formation of pores inside the hollow fibers, the length and the thickness of the fibers were increased. In contrast, the highly packed molecular chains induced by stretching tended to relax because of the strong interactions between the swelling agent and the blocks at elevated swelling temperatures, which would macroscopically lead to length reduction of the hollow fibers with high stretching percentages. With relatively low stretching percentages, the swelling effect had a major impact, while the stretching effect was insignificant; therefore, the length of the HFMs was increased significantly after swelling. However, with a constant increase in stretching percentage, the relaxation effect of the stretched hollow fibers was strengthened and played a dominating role compared to the swelling effect. Consequently, the lengths of the hollow-fiber membranes gradually declined with an increase stretching percentages. That is, the higher the stretching percentage, the larger is the length reduction after swelling.

With the formation of pores, the morphologies of the PSF-*b*-PEG hollow fibers changed significantly after swelling and were greatly related to the stretching percentage. As shown in Figure 4a, after swelling at 65 °C for 1 h, HFM-13% showed a generally porous morphology, but nonporous patches were also present on the outer surface. At the high spinning temperature of 200/210 °C, the mobility of both blocks were highly enhanced, and more PEG blocks were able to quickly migrate to the outermost surface of the fiber during spinning to come in direct contact with the spinneret wall, thus minimizing the energy-unfavorable contact of the more hydrophobic PSF blocks with the hydrophilic substrate (the spinneret wall).[31,32] In the following swelling treatment, the surface-tethered PEG chains may cover the pores generated by selective swelling in some local areas, giving the presence of nonporous patches. Strong stretching will reduce the thickness as well as the areal size of the surface-enriched PEG layer. Consequently, the hollow-fiber membranes prepared with the stretching percentage larger than 100% exhibited uniformly distributed pores without dense patchy areas on the outer surface (Figure 4b–f). Generally, all the cross sections of the PSF-*b*-PEG HFMs represented a bicontinuous porous structure after swelling (Figure S4), which was consistent with the morphology of the previously reported PSF-*b*-PEG flat-sheet membranes prepared by selective swelling.[24] In the selective swelling process, dimensional parameters of the hollow fibers (outer diameter, inner diameter, and wall thickness) were significantly increased because of the formation of pores at no expense of any composition of the BCP. As depicted in Table S1, the outer diameter, inner diameter, and wall thickness of HFM-13% were remarkably increased to 700, 369, and 166 μm from the initial values of 508, 276, and 116 μm before swelling, respectively. However, as can be obviously seen from Figure 4g–l, the dimensional parameters showed a decreased tendency with the

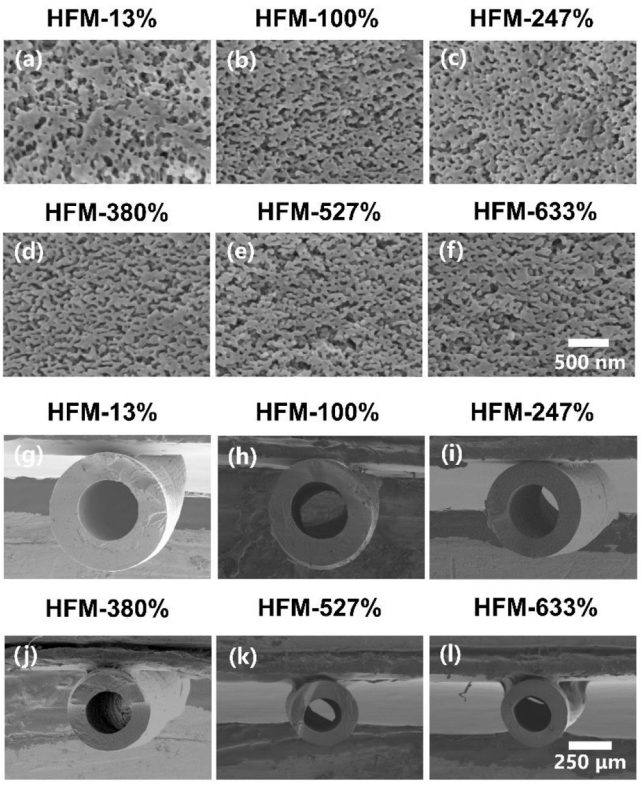

Figure 4. SEM images of the (a–f) outer surface and (g–l) cross section of the PSF-*b*-PEG HFMs prepared by selective swelling of the corresponding hollow fibers with different stretching percentages. (a–f) Same magnification and the scale bar is given in (f). (g–l) Same magnification and the scale bar is given in (l).

increased stretching percentage. With the stretching percentage of 100%, the outer diameter, inner diameter, and wall thickness of the hollow-fiber membrane were reduced to 663, 355, and 154 μm, respectively. These dimensional parameters further declined with the progressively increased stretching percentages. Nevertheless, it is observed from Table S1 that the decline of membrane thickness is not proportional. Membrane dimensions and wall thicknesses eventually reached a certain value with constantly increased stretching percentages (Figure 3b). Typically, the dimensional parameters of HFM-527% and HFM-633% were very close to each other after swelling. This is mainly due to the competition of volume expansion and the length shrink during selective swelling. Therefore, HFMs-527% with almost the thinnest wall thickness (98 μm), the smallest outer diameter (413 μm), and almost the maximum surface porosity is expected to exhibit the highest permeance.

3.3. Crystallization Behaviors of PSF-*b*-PEG Hollow Fibers Subjected to Stretching and Swelling. To better understand how the two blocks were influenced in the process of melt extrusion, stretching, and swelling, the crystallization behaviors of PEG phases restrained by the surrounded PSF matrix were studied. However, the PSF-*b*-PEG copolymer and their hollow fibers have already crystallized during the manufacturing process. It is impossible to real-time monitor the crystalline peaks ascribed to PEG during stretching and melt spinning, but the subsequent melting peaks can be used to well describe the crystallization process. Therefore, we analyzed the subsequent melting behaviors of PEG homopolymer, the PSF-*b*-PEG block copolymer, and PSF-*b*-PEG

https://doi.org/10.1021/acsapm.1c01882
ACS Appl. Polym. Mater. 2022, 4, 7989–7997

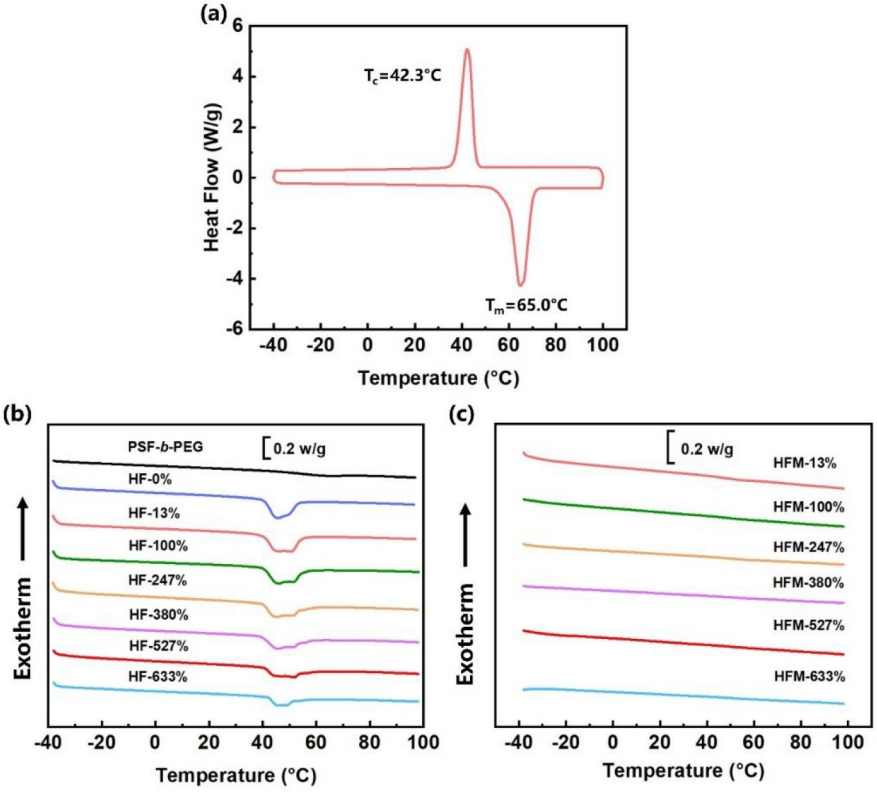

Figure 5. DSC curves of (a) the heating and cooling process for the PEG homopolymer, (b) the heating process for the PSF-*b*-PEG block copolymer and hollow fibers with various stretching percentages, and (c) the heating process for PSF-*b*-PEG HFMs after selective swelling. The scanning rate in all the DSC tests was 10 °C·min^{-1}.

hollow fibers with and without swelling treatment by means of DSC. As shown in Figure 5a, the PEG homopolymer showed an obvious melting peak at 65.0 °C during heating and a distinct crystallization peak at 42.3 °C during subsequent cooling at 10 °C·min^{-1}, indicating a relatively fast crystallization rate for PEG. However, no melting peak appeared in the heating traces of as-synthesized PSF-*b*-PEG granules (Figure 5b), implying that PEG phases in PSF-*b*-PEG hardly crystallized during the polymerization and purification process as a result of being restrained by the surrounded PSF blocks.[30] According to the findings in confined crystallization, the crystallization of PEG in block copolymers depends strongly on the weight fraction and the length of the PEG blocks as well as the degree of confinement.[33] Typically, the crystallization of polymers will be weakened when they are confined in the decreasing spaces, which leads to a stronger degree of confinement. Similarly, it has been previously reported that, when PVDF crystallized in the anodic alumina oxide (AAO) template with the pore diameter decreased to 30 nm, the crystallization of PVDF in the nanopores was largely restrained due to the strong confinement, and almost no melting peak was found in the heating trace.[34]

For the as-spun PSF-*b*-PEG hollow fibers, an intensive melting peak appeared at 49.4 °C, demonstrating that PEG was crystallized to a certain extent during the melt spinning process. However, the nascent hollow fiber (without additional stretching during melt spinning) exhibited a much lower melting peak (49.4 °C) and crystallinity (~23.4%) compared to those of the PEG homopolymer (65.0 °C and 78.4%, Table S2), suggesting that PEG formed a relatively loosely packed crystallite in the nascent fibers. This should be attributed to the confined effect posed by the glassy PSF matrix. This observation was also reported in other block copolymers such as poly(ethylene oxide)-*b*-polystyrene.[30,35] However, after being stretched by 13%, the fibers showed double melting peaks located at 45.4 and 50.8 °C, respectively. Moreover, the melting point and melting enthalpy were higher than those of nascent fibers, indicating that the crystallization of the PEG blocks was enhanced by stretching. With increasing stretching percentages, three melting points appeared for HF-247%, HF-380%, and HF-527%, implying that the PEG crystallization became more complicated. However, with the stretching percentage of 633%, the degree of crystallinity of the highly stretched fibers decreased because of the overstretching state of the PEG chains and the restriction of the stiff PSF skeleton. Importantly, the hollow fibers with and without additional stretching all displayed a much lower degree of crystallinity than that of the PEG homopolymer as a result of the confined effect of the PSF matrix. Besides, all the hollow fibers exhibited multiple melting behaviors as the crystallization of the PEG blocks is restrained in the PSF matrix. This phenomenon, originating from the thermal history, is commonly observed in DSC heating traces and is usually ascribed to the recrystallization/reorganization of the imperfect lamellae.[36,37]

We then investigated the crystallization state of PSF-*b*-PEG HFMs prepared by selective swelling in hot swelling agents. As can be seen from Figure 5c, no melting peak appeared in the DSC curves of the PSF-*b*-PEG HFMs prepared by stretching with different ratios followed by selective swelling, indicating that the PEG phases in these HFMs were changed to be in the amorphous state. In the selective swelling process performed at 65 °C, because of the strong interaction between the swelling

https://doi.org/10.1021/acsapm.1c01882
ACS Appl. Polym. Mater. 2022, 4, 7989−7997

agent and PEG, the PEG crystallites previously formed during the melt spinning and stretching were totally destroyed, leading to expanded phases of highly solvated PEG chains confined in the PSF matrix. In the subsequent drying step at room temperature, the swelling agent evaporated and the PEG chains were quickly condensed on the pore walls and film surfaces. These PEG chains were strongly confined to the surface (including pore walls) as the pores produced by selective swelling were only a few tens of nanometers in diameter; therefore, their crystallization was strongly restrained, and they were in the amorphous state.[34] Notably, the amorphous PEG segment migrated and collapsed onto the surface after swelling, resulting in inherently hydrophilic surfaces. This is highly desired to improve water permeance and to reduce membrane fouling.[24]

3.4. Separation Performance of PSF-*b*-PEG HFMs. Stretching greatly decreases the wall thickness of hollow-fiber membranes, and their water permeances are expected to be increased. Figure 6 displayed the water permeance and BSA

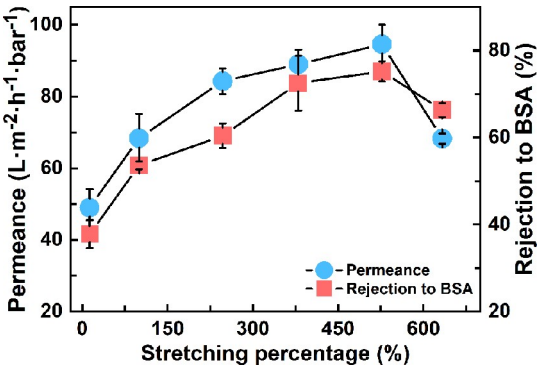

Figure 6. Permeance and BSA rejection of PSF-*b*-PEG HFMs with different stretching percentages.

rejection performance of PSF-*b*-PEG HFMs prepared at different stretching percentages. As expected, the water permeance was steadily increased from 49.0 to 94.6 L·m^{-2}·h^{-1}·bar^{-1} when the stretching percentage of the hollow fibers were increased from 13% to 527%. Notably, accompanied by the increase in water permeance, the rejection of the HFMs was also constantly increased from 37.8% for the HFM with slight stretching (HFM-13%) to 75.2% for the HFM with the stretching percentage of 527% (HFM-527%). That is, the water permeance and BSA rejection of PSF-*b*-PEG HFMs with optimal stretching treatment (HFM-527%) were simultaneously improved by multiple times. The improved water permeance is mainly due to the significant reduction in the wall thickness of the HFMs after stretching, resulting in a significant decrease in mass transfer resistance. Meanwhile, because of the small outer diameter of the hollow fibers subjected to strong stretching, there will be a stronger curvature effect in the swelling process and, consequently, the volume expansion caused by swelling will be weakened. That is, under the identical swelling condition, the PEG domains in these hollow fibers will be swollen to a less degree, and consequently, smaller pores will be generated. Therefore, HFMs prepared with higher stretching percentages possess smaller pores and, consequently, higher BSA rejections. However, when the stretching percentage was too high (HFM-633%), both the permeance and BSA rejection were decreased. This may be due to the fact that some defects were formed in the highly stretched hollow fibers and thus weakened the rejection of the membranes. Meanwhile, the generated pores were reduced to a significant degree, leading to a higher mass transfer resistance and consequently an obvious reduction in water permeance. Moreover, the higher stretching percentage represented the thinner wall thickness and weaker mechanical strength. Thus, some slight structural deformation might occur during performance testing and affected the membrane performance.

Compared with the BCP HFMs prepared by different processes, the performance of HFM-527% is moderate (Table S3).[1,10,12,38,39] We note that the water permeance of the HFMs prepared in this work still has room to improve mainly because the fiber walls have a symmetric structure posing large mass transfer resistance in the filtrations. Considering the "clean" nature of our process, which is less solvent-extensive and produces no wastewater, we believe it is worthwhile to put more effort in the improvement of the permeance of the thus-prepared hollow-fiber membranes. We are currently working to increase the water permeance of these BCP hollow-fiber membranes. A possible solution is to create gradient porosity in the fiber walls, thus lowering the transport resistance and subsequently improving water permeance at no cost of rejection. Also importantly, polymer design that optimizes the microstructure of block copolymers thus enabling the formation of denser and smaller pores by selective swelling is also expected to improve the membrane performance. Considering that selective swelling is capable of generating pores in a number of different block copolymers,[23] we believe that the process reported in this work can be adopted to prepare hollow-fiber membranes of other block copolymers when the copolymers are meltable, thus enabling melt spinning.

4. CONCLUSIONS

In summary, we report the preparation of PSF-*b*-PEG HFMs with improved separation performance based on a simple and efficient stretching process. We first melt-spin hollow fibers and adjust the wall thicknesses by axial stretching at different ratios. The stretched hollow fibers show gradually descending outer diameter, inner diameter, and wall thickness, while still maintaining the integral hollow structure even with a stretching percentage as high as 633%. Selective swelling is then used to generate pores in the stretched hollow fibers to produce HFMs. The lengths of the HFMs with higher stretching percentages gradually decrease as a result of relaxation of the oriented polymer chains. However, the thickness and outer diameter of the HFMs still decrease with an increase in stretching percentage and ultimately reach the minimum and stable value with a stretching percentage at 527% and above. During stretching and swelling, the crystallization state of the PEG phases is drastically changed. The crystallization of PEG blocks is promoted by the orientation effect and further adjusted by stretching. After selective swelling, crystals are destroyed; therefore, PEG chains are collapsed onto the surface in the amorphous state, leading to inherent hydrophilic surfaces. Under the optimized stretching condition, the permeance and BSA rejection of the PSF-*b*-PEG HFMs are increased synchronously as a result of the thinner fiber wall and smaller pore size.

https://doi.org/10.1021/acsapm.1c01882
ACS Appl. Polym. Mater. 2022, 4, 7989−7997

■ ASSOCIATED CONTENT

Supporting Information

The Supporting Information is available free of charge at https://pubs.acs.org/doi/10.1021/acsapm.1c01882.

Thermogravimetric curves of PSF-*b*-PEG; digital images of the hollow fibers; SEM images of the hollow fibers; SEM images of HFMs; parameters of HFMs; melting enthalpy and melting temperature of the hollow fibers; comparison of the performance of the BCP HFMs (PDF)

■ AUTHOR INFORMATION

Corresponding Authors

Shoutian Qiu − *State Key Laboratory of Materials-Oriented Chemical Engineering, College of Chemical Engineering, Nanjing Tech University, Nanjing 211816, P. R. China*; Email: qiust@njtech.edu.cn

Yong Wang − *State Key Laboratory of Materials-Oriented Chemical Engineering, College of Chemical Engineering, Nanjing Tech University, Nanjing 211816, P. R. China*; orcid.org/0000-0002-8653-514X; Email: yongwang@njtech.edu.cn

Authors

Dinglei Zhong − *State Key Laboratory of Materials-Oriented Chemical Engineering, College of Chemical Engineering, Nanjing Tech University, Nanjing 211816, P. R. China*

Jiemei Zhou − *State Key Laboratory of Materials-Oriented Chemical Engineering, College of Chemical Engineering, Nanjing Tech University, Nanjing 211816, P. R. China*

Dongwei Ma − *State Key Laboratory of Materials-Oriented Chemical Engineering, College of Chemical Engineering, Nanjing Tech University, Nanjing 211816, P. R. China*

Complete contact information is available at: https://pubs.acs.org/10.1021/acsapm.1c01882

Notes

The authors declare no competing financial interest.

■ ACKNOWLEDGMENTS

Financial support from the Key Research and Development Program of Jiangsu Province (BE2021714) and the National Natural Science Foundation of China (21825803, 22108117) is gratefully acknowledged.

■ REFERENCES

(1) Sankhala, K.; Koll, J.; Abetz, V. Setting the stage for fabrication of self-assembled structures in compact geometries: Inside-out isoporous hollow-fiber membranes. *ACS Macro Lett.* **2018**, *7* (7), 840−845.

(2) Huang, Y.; Xiao, C.; Huang, Q.; Liu, H.; Zhao, J. Progress on polymeric hollow-fiber membrane preparation technique from the perspective of green and sustainable development. *Chem. Eng.J.* **2021**, *403*, 126295.

(3) Peng, N.; Widjojo, N.; Sukitpaneenit, P.; Teoh, M. M.; Lipscomb, G. G.; Chung, T.-S.; Lai, J.-Y. Evolution of polymeric hollow fibers as sustainable technologies: Past, present, and future. *Prog. Polym. Sci.* **2012**, *37* (10), 1401−1424.

(4) Zhou, F.; Tien, H. N.; Xu, W. L.; Chen, J.-T.; Liu, Q.; Hicks, E.; Fathizadeh, M.; Li, S.; Yu, M. Ultrathin graphene oxide-based hollow-fiber membranes with brush-like CO_2-philic agent for highly efficient CO_2 capture. *Nat. Commun.* **2017**, *8* (1), 2107.

(5) Paul, D. Polymer hollow-fiber membranes for removal of toxic substances from blood. *Prog. Polym. Sci.* **1989**, *14*, 597−627.

(6) Lau, H. S.; Yong, W. F. Recent progress and prospects of polymeric hollow-fiber membranes for gas application, water vapor separation and particulate matter removal. *J. Mater.Chem.A* **2021**, *9* (47), 26454−26497.

(7) Zhao, J.; Shi, L.; Loh, C. H.; Wang, R. Preparation of PVDF/PTFE hollow-fiber membranes for direct contact membrane distillation *via* thermally induced phase separation method. *Desalination* **2018**, *430*, 86−97.

(8) Mun, J.; Park, H. M.; Koh, E.; Lee, Y. T. Enhancement of the crystallinity and surface hydrophilicity of a PVDF hollow-fiber membrane on simultaneous stretching and coating method. *J. Ind.Eng. Chem.* **2018**, *65*, 112−119.

(9) Jeon, S.; Karkhanechi, H.; Fang, L.-F.; Cheng, L.; Ono, T.; Nakamura, R.; Matsuyama, H. Novel preparation and fundamental characterization of polyamide 6 self-supporting hollow-fiber membranes via thermally induced phase separation (TIPS). *J. Membr. Sci.* **2018**, *546*, 1−14.

(10) Sankhala, K.; Koll, J.; Radjabian, M.; Handge, U. A.; Abetz, V. A pathway to fabricate hollow-fiber membranes with isoporous inner surface. *Adv.Mater. Interfaces* **2017**, *4* (7), 1600991.

(11) Noor, N.; Koll, J.; Abetz, C.; Notzke, H.; Abetz, V. Continuous production of macroporous films: an alternative to breath figure assembly. *Sci. Rep.* **2017**, *7* (1), 8050.

(12) Liu, Y.; Liu, T.; Su, Y.; Yuan, H.; Hayakawa, T.; Wang, X. Fabrication of a novel PS4VP/PVDF dual-layer hollow fiber ultrafiltration membrane. *J. Membr. Sci.* **2016**, *506*, 1−10.

(13) Komaladewi, A. A. I. A. S.; Anisah, S.; Wardani, A. K.; Surata, I. W.; Subagia, I. D. G. A.; Wenten, I. G. The effect of annealing and stretching parameters on the structure and performance of polypropylene hollow-fiber membrane. *Mater. Res. Express* **2019**, *6* (5), 054001−054009.

(14) Kim, J.-J.; Jang, T.-S.; Kwon, Y.-D.; Kim, U. Y.; Kim, S. S. Structural- study of microporous polypropylene hollow-fiber membranes made by the melt-spinning and cold-stretching method. *J. Membr. Sci.* **1994**, *93*, 209−215.

(15) Ji, D.; Xiao, C.; An, S.; Chen, K.; Gao, Y.; Zhou, F.; Zhang, T. Completely green and sustainable preparation of PVDF hollow-fiber membranes via melt-spinning and stretching method. *J. Hazard. Mater.* **2020**, *398*, 122823.

(16) Figoli, A.; Marino, T.; Simone, S.; Di Nicolò, E.; Li, X. M.; He, T.; Tornaghi, S.; Drioli, E. Towards non-toxic solvents for membrane preparation: a review. *Green Chem.* **2014**, *16* (9), 4034−4059.

(17) Luo, D.; Xie, G.; Qin, S. The hydrophilic polypropylene/poly(ethylene-co-vinyl alcohol) hollow-fiber membrane with bimodal microporous structure prepared by melt-spinning and stretching. *Sep. Purif. Technol.* **2021**, *274*, 118890.

(18) Kim, J.; Kim, S. S.; Park, M.; Jang, M. Effects of precursor properties on the preparation of polyethylene hollow-fiber membranes by stretching. *J. Membr. Sci.* **2008**, *318* (1−2), 201−209.

(19) Zhao, X.; Zhang, R.; Liu, Y.; He, M.; Su, Y.; Gao, C.; Jiang, Z. Antifouling membrane surface construction: Chemistry plays a critical role. *J. Membr. Sci.* **2018**, *551*, 145−171.

(20) Zhong, D.; Zhou, J.; Wang, Y. Hollow-fiber membranes of block copolymers by melt spinning and selective swelling. *J. Membr. Sci.* **2021**, *632*, 119374.

(21) Wang, Y.; Li, F. An emerging pore-making strategy: confined swelling-induced pore generation in block copolymer materials. *Adv. Mater.* **2011**, *23* (19), 2134−2148.

(22) Wang, Y. Nondestructive creation of ordered nanopores by selective swelling of block copolymers: toward homoporous membranes. *Acc. Chem. Res.* **2016**, *49* (7), 1401−1408.

(23) Zhou, J.; Wang, Y. Selective swelling of block copolymers: An upscalable greener process to ultrafiltration membranes? *Macromolecules* **2020**, *53*, 5−17.

(24) Wang, Z.; Liu, R.; Yang, H.; Wang, Y. Nanoporous polysulfones with in situ PEGylated surfaces by a simple swelling strategy using paired solvents. *Chem. Commun.* **2017**, *53* (65), 9105−9108.

(25) He, B.; Tian, L.; Li, J.; Pan, Z. Effect of hot-stretching on morphology and mechanical properties of electrospun PMIA nanofibers. *Fibers Polym.* **2013**, *14* (3), 405−408.
(26) Song, Z.; Hou, X.; Zhang, L.; Wu, S. Enhancing crystallinity and orientation by hot-stretching to improve the mechanical properties of electrospun partially aligned polyacrylonitrile (PAN) nanocomposites. *Materials* **2011**, *4* (4), 621−632.
(27) Debbabi, F.; Abdessalem, S. B. Impact of hot-stretching treatment on physical and mechanical properties of braided polyamide suture. *Text. Res. J.* **2016**, *86* (7), 696−709.
(28) Leal, A. A.; Best, J. P.; Rentsch, D.; Michler, J.; Hufenus, R. Spectroscopic elucidation of structure-property relations in filaments melt-spun from amorphous polymers. *Eur. Polym. J.* **2017**, *89*, 78−87.
(29) Zhong, D.; Wang, Z.; Lan, Q.; Wang, Y. Selective swelling of block copolymer ultrafiltration membranes for enhanced water permeability and fouling resistance. *J. Membr. Sci.* **2018**, *558*, 106−112.
(30) Chen, S.; Wang, L. Confined crystallization kinetics and scale of semicrystalline block copolymer via non-isothermal method. *J. Therm. Anal. Calorim.* **2017**, *127* (3), 2341−2351.
(31) Yin, J.; Yao, X.; Liou, J.-Y.; Sun, W.; Sun, Y.-S.; Wang, Y. Membranes with highly ordered straight nanopores by selective swelling of fast perpendicularly aligned block copolymers. *ACS Nano* **2013**, *7* (11), 9961−9974.
(32) Sun, W.; Wang, Z.; Yao, X.; Guo, L.; Chen, X.; Wang, Y. Surface-active isoporous membranes nondestructively derived from perpendicularly aligned block copolymers for size-selective separation. *J. Membr. Sci.* **2014**, *466*, 229−237.
(33) Müller, A. J.; Balsamo, V.; Arnal, M. L. Nucleation and crystallization in diblock and triblock copolymers. *Adv. Polym. Sci.* **2005**, *190*, 1−63.
(34) Dai, X.; Niu, J.; Ren, Z.; Sun, X.; Yan, S. Effects of nanoporous anodic alumina oxide on the crystallization and melting behavior of poly(vinylidene fluoride). *J. Phys. Chem. B* **2016**, *120* (4), 843−50.
(35) Huang, P.; Zhu, L.; Guo, Y.; Ge, Q.; Jing, A. J.; Chen, W. Y.; Quirk, R. P.; Cheng, S. Z. D.; Thomas, E. L.; Lotz, B.; Hsiao, B. S.; Avila-Orta, C. A.; Sics, I. Confinement size effect on crystal orientation changes of poly(ethylene oxide) blocks in poly(ethylene oxide)-*b*-polystyrene diblock copolymers. *Macromolecules* **2004**, *37*, 3689−3698.
(36) Zhu, H.; Yang, H.; Zhao, Y.; Wang, D. The dynamic crystallization and multiple melting behavior of polypropylene in the in-reactor alloy: a differential scanning calorimetry study. *J. Appl. Polym. Sci.* **2011**, *121* (3), 1372−1383.
(37) Papageorgiou, G. Z.; Bikiaris, D. N.; Achilias, D. S.; Nanaki, S.; Karagiannidis, N. Synthesis and comparative study of biodegradable poly(alkylene sebacate)s. *J. Polym. Sci., Part B: Polym. Phys.* **2010**, *48* (6), 672−686.
(38) Hilke, R.; Pradeep, N.; Madhavan, P.; Vainio, U.; Behzad, A. R.; Sougrat, R.; Nunes, S. P.; Peinemann, K. V. Block copolymer hollow fiber membranes with catalytic activity and pH-response. *ACS Appl. Mater. Interfaces* **2013**, *5*, 7001−7006.
(39) Hilke, R.; Pradeep, N.; Behzad, A. R.; Nunes, S. P.; Peinemann, K.-V. Block copolymer/homopolymer dual-layer hollow fiber membranes. *J. Membr. Sci.* **2014**, *472*, 39−44.

https://doi.org/10.1021/acsapm.1c01882
ACS Appl. Polym. Mater. 2022, 4, 7989−7997